Asian Journal of Chemistry; Vol. 37, No. 9 (2025), 2211-2226
ASIAN JOURNAL OF CHEMISTRY
https://doi.org/10.14233/ajchem.2025.34158

Integrated Approach: Synthesis, *in vitro* Evaluation and Computational Analysis of Bromoanilines as Potential Antioxidants

NARUTI LONGKUMER[1,2], KIKOLEHO RICHA[3], RITUPARNA KARMAKER[1,2], BASANTA SINGHA[1], BENZIR AHMED[4], PENLISOLA LONGKUMER[1], PARTHA PRATIM GOGOI[1], NICHAN BORUAH[1], RITURAJ BARMAN[4], BIPUL BEZBARUAH[4] and UPASANA BORA SINHA[1,*]

[1]Department of Chemistry, Nagaland University, Lumami-798627, India
[2]Department of Chemistry, St. John College, Dimapur-797112, India
[3]Department of Biotechnology, St. Joseph University, Chumoukedima-797115, India
[4]Department of Applied Sciences, Gauhati University, Guwahati-781014, India

*Corresponding author: E-mail: upasanabsinha@gmail.com

Received: 30 May 2025 *Accepted*: 6 August 2025 *Published online*: 30 August 2025 AJC-22101

Bromoanilines are pivotal in medicinal chemistry, serving as crucial intermediates for bioactive compounds like antioxidants and therapeutic agents. Despite their potential, their intrinsic properties remain underexplored. This study innovatively synthesized bioactive bromoanilines using a greener protocol with water as the solvent and cetyltrimethylammonium tribromide (CTMATB) as the brominating agent, chosen for its sustainable characteristics. The synthesized compounds were evaluated for their antioxidant activity using DPPH, where 4-bromo-2-nitroaniline (**3a**) demonstrated exceptional activity with an IC_{50} of 1.73 mg/mL, surpassing Trolox as a positive control. FRAP assay further validated the superior antioxidant behaviour of compound **3a**. In-depth analysis *via* density functional theory (DFT) highlighted antioxidant mechanisms, favouring the sequential proton loss electron transfer (SPLET) pathway. Molecular docking with myeloperoxidase (MPO) with PDB ID: 1DNU underscored **3a**'s strong affinity, with a Moldock score of -54.98 kcal/mol. Further analyses through visual molecular dynamics (VMD), non-covalent interaction (NCI) and electron localization function (ELF), confirmed its stable interactions and electron distribution. Physico-chemical assessments underscored favourable drug-like profile and safety compound **3a**. This comprehensive approach reveals 4-bromo-2-nitroaniline (**3a**) as a promising antioxidant with potential therapeutic applications. However, further studies including *in vivo* exploration and clinical trials are crucial to validate its efficacy and safety as an antioxidant.

Keywords: Bromoanilines, Antioxidants, DFT, Molecular docking, ADMET.

INTRODUCTION

The importance of antioxidants has been gaining interest as oxidative metabolism is crucial for cell survival [1]. This metabolic process generates free radicals and other reactive oxygen species (ROS) which are attributed to the pathogenesis of various diseases, including diabetes, heart failure, cancer, atherosclerosis, inflammation and Alzheimer's by causing oxidative damage [2-4]. Antioxidants are chemical compounds that can react with free radicals and prevent oxidative damage of biomolecules and are therefore employed in the treatment of such widespread diseases [2,5]. Designing a novel synthetic protocol involves new reaction methodologies tested on the selection of suitable substrates known as test substrates with relevant reactivity, affordability and easy availability. In recent years, different types of bromo organic compounds have been synthesized using diverse organic transformations like substitution [6-10], oxidation [11-14], catalysis [15-17], co-halogenation [18-21] and rearrangement reactions [22,23], *etc.*

Our research interest on synthesizing various quaternary ammonium tribromides has resulted in a series of brominated compounds with diverse functionalities, which had not been previously investigated for their biological properties like anticancer [24-27], antioxidant [28-31], antimicrobial [29,32-36], antitubercular [29,37], cytotoxic [38] activities, *etc*. However, despite numerous reports on the synthesis of bromoanilines for various applications, it has been observed that these small

molecules are not considered for further studies to test their intrinsic properties [39-43]. Our earlier investigation focused on the antimicrobial properties of certain small bromo organic compounds, including bromoanilines; herein, we delved into the antioxidant potentials of some selected bromoanilines [32]. Evidently, certain compounds exhibit dual functionality as antibacterial agents and antioxidants by interacting with crucial bacterial cellular processes and possessing antioxidative properties which protects against oxidative stress-induced damage [44-46]. This dual activity is due to their selective generation of reactive oxygen species (ROS), inducing bacterial specific oxidative stress while safeguarding host cells, facilitated by variances in redox states and antioxidant defense mechanisms. For example, rutin from *Citrus sinensis* peels demonstrated synergistic effects with gentamicin against multidrug-resistant *P. aeruginosa*, inhibiting biofilm development through ROS-induced oxidative stress, disrupting the cell wall and eradicating bacteria [47]. Similarly, stilbenes cause cell membrane damage, oxidative stress-mediated DNA degradation, increased membrane permeability and release of intracellular components, contributing to antimicrobial action [48-52]. Beyond phenolic compounds like flavonoids and polyphenols, natural products such as essential oils [53], quinone compounds [54,55] selenium-containing compounds, *etc.* also exhibit antibacterial and antioxidant properties by triggering ROS-mediated oxidative stress within bacterial cells, leading to bacterial demise [56].

Although *in vitro* studies demonstrate that the dual activities, effectiveness and mechanisms can vary due to compound specificity, bacterial strains, experimental conditions and other factors. Further investigations, including *in vivo* and clinical trials, are crucial for validating the therapeutic potential of these compounds. It has been noted that for the structural studies, density functional theory (DFT) is a useful tool for identifying modes of action, reaction mechanisms, *etc.* [28,57-60]. Antioxidant compounds works through several mechanisms such as HAT, SET-PT, SPLET and chelation of transition metals [59,61,62]. Another sophisticated computational approach for comprehending receptor-ligand interactions is molecular docking [63-65], which is therefore integrated in this study. Docking simulations were performed with a myeloperoxidase (MPO) enzyme (PDB id: 1DNU) to assess possible interaction with the antioxidant compounds. Myeloperoxidase (MPO) plays a significant role as a target for antioxidant activity due to its involvement in oxidative stress and inflammation [66]. MPO is an enzyme found predominantly in immune cells, such as neutrophils, monocytes and macrophages [67]. It generates reactive oxygen species (ROS) including hypochlorous acid (HOCl) as part of the immune response to combat microbial infections [68]. Thus, by targeting myeloperoxidase enzyme with inhibitors can effectively defend against oxidative stress damage. Furthermore, to investigate the underlying mechanisms of interaction between the compounds and the target enzyme amino acid residues, we carried out a theoretical study employing the quantum mechanical DFT analysis. Non-covalent interaction (NCI) analysis was implemented to gain a comprehensive understanding of the interaction between the compounds and amino acids of the target protein. We utilized visual molecular dynamics (VMD) to visualize the probable interacting sites within the most favoured antioxidants-amino acid complexes. Also, electron localized function (ELF) analysis was performed to observe changes in electron density with both individual and interacted compounds-amino acid complexes [69-72]. Screening of the physico-chemical attributes, medicinal effects and toxicity parameters provides a deeper understanding of the druglike characteristics which can aid in evaluating their suitability for therapeutic applications. Thus, these studies can collectively enhance our understanding of molecule behaviour and interactions in diverse chemical and biological systems [73].

EXPERIMENTAL

Chemicals used in the study were procured from various commercial suppliers like Sigma-Aldrich, Merck and S.D. Fine Chem., India. They were employed without further purification. The reactions were performed utilizing a single-mode microwave reactor, the CATA 2R from Catalyst System (Pune, India). Characterization of the products was conducted through various spectroscopic techniques including IR spectra, mass spectra and NMR spectra. The IR spectra were recorded using a Perkin-Elmer FT-IR instrument (spectrum 2) with KBr pellets. Proton and carbon NMR spectra were obtained using a JEOL-EC 400 instrument, employing $CDCl_3$ as the solvent. Mass spectra were acquired using an Inkarp mass spectrophotometer (APCI).

Synthesis of bromoanilines: Bromoanilines were synthesized through facile green method as reported earlier [32] where cetyltrimethylammonium tribromide (CTMATB) was used for the bromination of substrates. The reaction takes place in a single mode microwave reactor (CATA 2R) at a controlled power of 595 W (**Scheme-I**). To eliminate the use of harmful organic solvents, this methodology employs water as solvent. The products were obtained *via* column chromategraphy using silica gel.

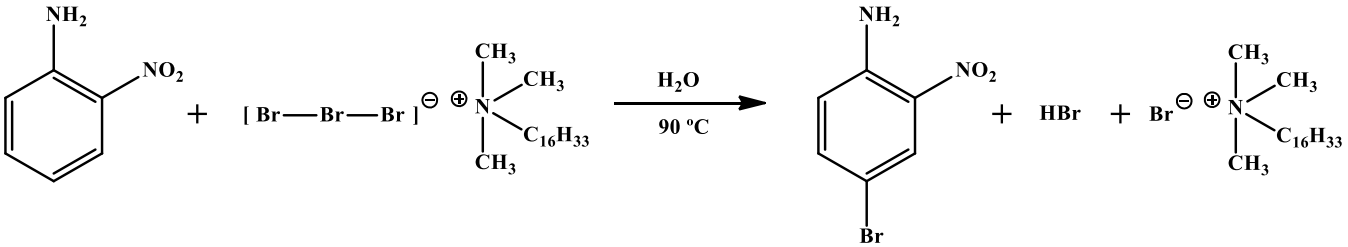

Scheme-I: Reaction of 2-nitroaniline with CTMATB to give 4-bromo-2-nitroaniline (**3a**)

Spectral data

2-Bromo-4-iodoaniline (2a): ^{1}H NMR (400 MHz, $CDCl_3$) δ ppm: 3.84 (brs, 2H), 6.63 (d, J = 7.8 Hz, H), 7.32 (dd, J_1 = 7.6 Hz, J_2 = 1.6 Hz, H), 7.51 (d, J = 1.6 Hz H); ^{13}C NMR (100 MHz, $CDCl_3$): δ 78.30, 109.97, 117.28, 131.11, 139.89, 143.80; IR (KBr, ν_{max}, cm^{-1}): 3393, 3290, 3170, 1612, 1555, 1470, 1256, 608, 535.

4-Bromo-*o*-toluidine (4a): ^{1}H NMR (400 MHz, $CDCl_3$) δ ppm: 2.16 (s, 3H), 4.04 (brs, 2H), 7.10 (d, J = 7.8 Hz, H), 7.40 (dd, J_1 = 7.8 Hz, J_2 = 2.0 Hz, H), 7.41 (d, J = 2.0 Hz, H); ^{13}C NMR (100 MHz, $CDCl_3$): δ 18.16, 109.36, 118.82, 124.88, 131.02, 131.92, 141.45; IR (KBr, ν_{max}, cm^{-1}): 3481, 3340, 3072, 1615, 1584, 1468, 1443, 1282, 548.

4-Bromo-*m*-toluidine (5a): ^{1}H NMR (400 MHz, $CDCl_3$) δ ppm: 2.25 (s, 3H), 4.12 (brs, 2H), 6.52 (d, J = 8.2 Hz, H), 7.24 (dd, J_1 = 8.2, J_2 = 2.5 Hz, H), 7.52 (d, J = 2.5 Hz, H); ^{13}C NMR (100 MHz, $CDCl_3$): δ ppm: 24.11, 112.39, 113.99, 131.34, 134.73, 137.80, 143.72; IR (KBr, ν_{max}, cm^{-1}): 3472, 3378, 3045, 1609, 1454, 1407, 1256, 563.

3-Bromo-2,4-dimethylaniline (7a): ^{1}H NMR (400 MHz, $CDCl_3$) δ 2.17 (s, 3H), 2.19 (s, 3H), 6.80 (d, J = 8.3 Hz, H), 7.11 (d, J = 8.2 Hz, H); ^{13}C NMR (100 MHz, $CDCl_3$): δ ppm: 18.27, 20.04, 109.35, 123.43, 128.37, 130.24, 130.31, 139.64; IR (KBr, ν_{max}, cm^{-1}): 3403, 3306, 3051, 1622, 1598, 1564, 1486, 1376, 1288, 560.

2,2-Diphenyl-1-picrylhydazyl (DPPH) radical scavenging assay: The DPPH radical scavenging activity of the synthesized compounds was investigated using the method of Mentese *et al*. [2] with minor alterations. Different concentrations of compound (1 mL each) were added to 3 mL of 0.1 mM DPPH solution. The mixtures were vortexed and allowed to stand in the dark at room temperature for 30 min. Following incubation, each reaction mixture was measured for absorbance at 517 nm in a UV-Vis spectrophotometer (Perkin Elmer Lambda 365). Trolox was used as the standard and methanol was run as blank. The percentage of free radicals that the test compounds were able to inhibit was used to express their radical scavenging activity and was calculated as:

$$\text{DPPH scavenging effect (\%)} = \frac{A_0 - A_1}{A_0} \times 100$$

where A_0 = absorbance of control (blank), A_1 = absorbance of the test compounds.

Tests were run in threefold and the outcomes were calculated as mean values ± standard errors.

FRAP assay: The reducing power assay was studied using the methodology as described by Oyaizu [74]. The compounds at different concentrations were added to 2.25 mL of phosphate buffer (0.2 M, pH 6.6) and 2.5 mL of potassium ferricyanide (1%). After an incubation period of 20 min at 50 ºC, 2.5 mL of 10% w/v trichloroacetic acid (TCA) was added and the mixture was centrifuged for 10 min at 700 rpm. 0.5 mL ferric chloride (0.1%) and 2.5 mL distilled water were added after the upper layer of the solution (2.5 mL) was taken out. A UV-Vis spectrophotometer (Perkin Elmer Lambda 365) was used to record the absorbance of the final solution mixture at 700 nm. High absorbance indicates that the test compounds have greater reducing power. Tests were executed in triplicate and the findings were presented as mean values ± standard errors; Trolox was the standard used for the study.

Computational studies: The DFT studies were performed using Gaussian 09 [75] software. After optimization, all structures were built and visualized using the graphical user interface GaussView5 [76]. Because of its careful balance of computational cost and result precision, the compounds were optimized using the hybrid functional B3LYP [76,77] and the basis set LANL2DZ was used to optimize all the involved structures. Following optimization, the structures were then examined further to compute their vibrational frequencies, which indicated the characteristics of the stationary points. The polarizable continuum model was applied with DMSO (ε = 47.24), since the experimental studies were conducted in DMSO as the solvent. The calculated enthalpy of $H^{\bullet}$ and H^+ predicted using the B3LYP/LANL2DZ method in DMSO was -1303.56 kJ/mol and -421.92 kJ/mol, respectively. The solvation enthalpy of e^- was taken from reference [78].

Bond dissociation enthalpy (BDE) is a vital factor in determining the HAT mechanism of antioxidant activity [79-82]. A lower bond dissociation enthalpy value corresponds to better antioxidant activity [79] and the BDE was calculated using the following equation:

$$BDE = H(R^{\bullet}) + H(H^{\bullet}) - H(R{-}H) \quad (1)$$

To understand the SET-PT mechanism, the dissociation enthalpy (PDE) and ionization potential (IP) proton energy factors were calculated as follows:

$$IP = H(R{-}H^{\bullet+}) + H(e^-) - H(R{-}H) \quad (2)$$

$$PDE = H(R^{\bullet}) + H(H^+) - H(R{-}H^{\bullet+}) \quad (3)$$

here, $H(R{-}H^{\bullet+})$ = enthalpy of R-H radical cation; $H(e^-)$ = enthalpy of single electron.

The electron transfer enthalpy (ETE) and proton affinity (PA) parameters define the SPLET mechanism. The ETE and PA were estimated using the calculations below:

$$PA = H(R^-) + H(H^+) - H(R{-}H) \quad (4)$$

$$ETE = H(R^{\bullet}) + H(e^-) - H(R^-) \quad (5)$$

here, $H(R^-)$ = Enthalpy of R ion; $H(H^+)$ = enthalpy of H ion.

Thus, in this work the HAT, SET-PT and SPLET mechanisms were studied to understand the mode of scavenging activity of the compounds under study.

Molecular docking studies: Molecular docking studies were conducted to gain a comprehensive understanding of the binding interactions between the synthesized bromoaniline compounds and the target protein MPO. The Molegro Virtual Docker (MVD) software was utilized for docking the bromoaniline compounds into the active site of MPO (PDB ID: 1DNU) [83]. The MPO protein structure in PDB file format was obtained from the Research Collaboratory for Structural Bioinformatics (RCSB) Protein Data Bank (http://www.rcsb.org/). The 3D structures of the ligands were generated using ChemBio3D Ultra 12.0, optimized using the MM2 force field and saved as mol2 files. During the docking procedure, water molecules were excluded and charges were assigned to the protein. MVD was employed to identify cavities and the binding site was defined with a radius of 15 Å, centred at X: 28.29, Y: -12.25, Z: 7.67, with a volume of 103.94 $Å^3$ and a surface area of 389.12 $Å^2$. Docking simulations were perfor-

med and each ligand underwent 30 independent runs. For the analysis of molecular interactions, particularly hydrogen bonding, the top pose of each ligand based on the docking score was selected [84,85].

Analysis of electron localized function (ELF), visual molecular dynamics (VMD) and non-covalent interaction (NCI): Non-covalent interaction (NCI), visual molecular dynamics (VMD) and reduced density gradient (RDG) analyses enable the visualization and understanding of potential interaction sites between different molecular entities [69-71]. In this study, the NCI-RDG analysis was performed using the multifunctional wavefunction analyzer software (Multiwfn) to determine the preferred interaction sites within a minimized compound-alanine/threonine/glycine complex [72]. Additionally, the electron localization function (ELF) analysis was employed to examine the variations in electron cloud density of molecules before and after interaction, providing valuable insights into the system [86]. Computational probes for ADMET properties, encompassing the physico-chemical attributes, medicinal effects and toxicity parameters, contribute significantly to understand the intrinsic antioxidant activity of bromoanilines, assisting in determining their therapeutic uses [87].

RESULTS AND DISCUSSION

Over the years, significant efforts have been directed towards adopting greener solvents, with water emerging as the greenest option due to its abundance, non-corrosive, non-flammable and non-toxic properties [88,89]. Consequently, water was utilized as the solvent for the present bromination reactions. To address the limitations associated with using water as a solvent, these aqueous reactions were conducted in a microwave reactor, which also serves to accelerate the reaction process. Quaternary ammonium tribromides (QATBs) have been identified as greener alternatives for bromination, with reports indicating that cetyltrimethylammonium tribromide (CTMATB) is the superior brominating agent among QATBs [77]. Therefore, CTMATB was selected as the reagent of choice. The use of CTMATB in aqueous reactions provides an eco-friendly approach to the bromination of organic molecules. The outcomes of the microwave-assisted bromination reactions are presented in Table-1, demonstrating that the products were obtained in good yields [90].

DPPH radical scavenging assay: The radical scavenging activities of the synthesized compounds at various concentrations were evaluated using DPPH, with Trolox serving as the positive control. The results are presented in Table-2 and Fig. 1. This assay is based on the compound's ability to donate hydrogen atoms or scavenge free radicals, thereby neutralizing the radical nature of DPPH [91]. The reduction in absorbance of DPPH radicals at 517 nm, induced by antioxidants, was measured to assess their reduction capacity. All the tested compounds exhibited antioxidant activity, with IC_{50} values ranging from 1.73 mg/mL to 5.13 mg/mL. Among the compounds studied, compounds **2a** and **3a** demonstrated superior antioxidant activity. These findings suggest that electron-withdrawing groups, such as iodine and nitro substituents, may enhance antioxidant activity.

TABLE-1
MICROWAVE ASSISTED BROMINATION
WITH CTMATB IN AQUEOUS CONDITION

Substrate	Product	Yield (%)
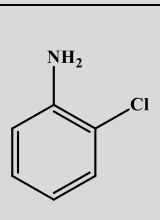	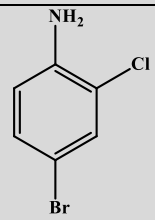 **(1a)** [32]	66
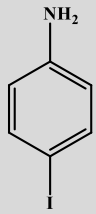	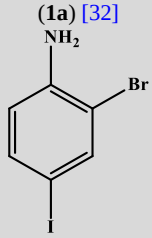 **(2a)**	73
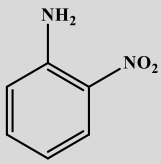	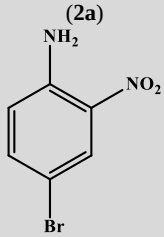 **(3a)** [32]	60
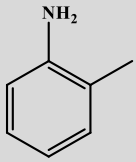	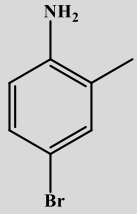 **(4a)**	85
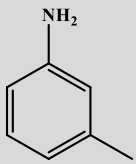	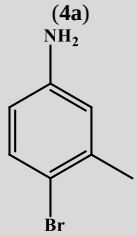 **(5a)**	62
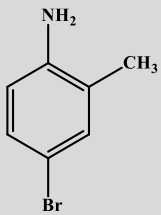	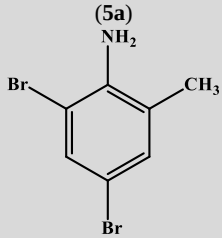 **(6a)** [32]	71
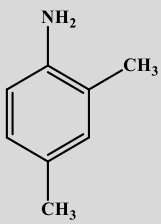	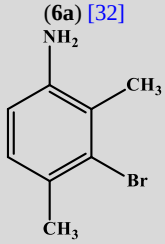 **(7a)**	91

TABLE-2
DPPH RADICAL SCAVENGING ACTIVITY OF THE SYNTHESIZED BROMOANILINES

Compound	IC_{50} (mg/mL)	Compound	IC_{50} (mg/mL)
1a	3.13 ± 0.2	**5a**	4.56 ± 0.3
2a	1.82 ± 0.2	**6a**	5.13 ± 0.3
3a	1.73 ± 0.3	**7a**	2.04 ± 0.2
4a	4.14 ± 0.4	Trolox	1.05 ± 0.2

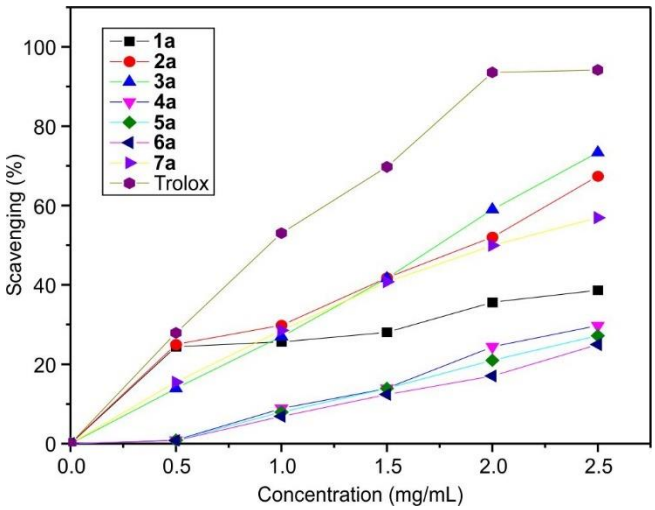

Fig. 1. DPPH radical scavenging activity of the synthesized bromoanilines

FRAP assay: The antioxidant behaviour of the synthesized compounds was evaluated using the FRAP assay, with the results depicted in Fig. 2. This assay measures antioxidant activity based on a compound's ability to reduce ferric ions (Fe^{3+}) to ferrous ions (Fe^{2+}), resulting in a colour change from yellow to green or blue, which indicates the intensity of the reduction ability [61,92]. The absorbance of the compounds was measured at a wavelength of 700 nm using a spectrophotometer. Fig. 2 clearly shows that compound **3a** exhibited the superior antioxidant behaviour compared to the other compounds. This compound not only demonstrated the highest reduction ability but also the most pronounced colour change,

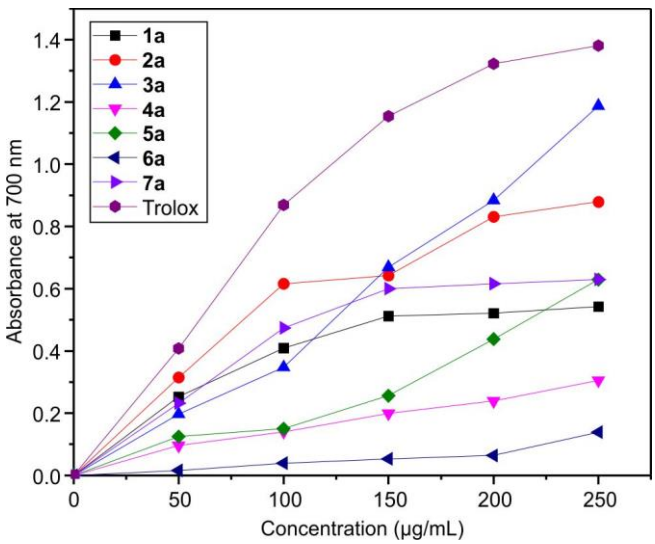

Fig. 2. Reducing power activity of the synthesized bromoanilines by FRAP assay

indicating its potent antioxidant properties. Furthermore, compound **3a** exhibited the highest radical scavenging activity within the series, suggesting that its molecular structure effectively enhances its capacity to neutralize free radicals. These findings highlight the potential of compound **3a** as a strong antioxidant agent.

Computational studies: Density functional theory (DFT) studies have been employed to gain a deeper understanding of the mechanistic behaviour underlying the antioxidant activity of the synthesized compounds. The hydrogen atom transfer (HAT), single-electron transfer-proton transfer (SET-PT) and sequential proton loss electron transfer (SPLET) mechanisms were explored by analyzing the bond dissociation enthalpy (BDE), ionization potential (IP), proton dissociation enthalpy (PDE), proton affinity (PA) and electron transfer enthalpy (ETE) values at all possible N-H and C-H positions, as detailed in Table-3. The results reveal the following order for the BDE values: **3a** < **1a** < **5a** < **6a** ≈ **7a** < **4a** < **2a**. For the IP values, the order is **3a** < **1a** < **2a** < **6a** < **5a** < **4a** < **7a**. The PDE values are ordered as **7a** < **5a** < **4a** < **6a** < **2a** < **1a** < **3a**. The PA values follow the sequence **3a** < **1a** < **5a** < **2a** < **6a** < **4a** < **7a** and the ETE values are arranged in the order **3a** < **5a** < **1a** < **2a** < **6a** < **4a** < **7a**. Notably, the PA values are the lowest among the studied parameters, suggesting that the SPLET mechanism is more favourable for these compounds. The SPLET mechanism involves the initial loss of a proton (proton dissociation) followed by an electron transfer. This process is particularly efficient in compounds where the N-H bonds exhibit lower PA and ETE values, indicating that the amine groups are proficient at losing a proton and transferring an electron.

The prominence of low PA and ETE values for N-H bonds implies that these sites are highly conducive to the SPLET mechanism. This mechanism is advantageous since it allows the antioxidant to efficiently neutralize free radicals by first donating a proton and subsequently an electron, thereby stabilizing the radical species. The data suggests that compound **3a**, with its favourable BDE, IP, PA and ETE values, is particularly effective in engaging in the SPLET mechanism, which may account for its superior antioxidant activity as observed in the experimental assays. This insight into the mechanistic pathways underscores the potential of amine-containing compounds in antioxidant applications, highlighting their efficiency in proton and electron transfer processes.

Molecular docking studies: The binding mechanism of the synthesized bromoanilines was investigated using myeloperoxidase (MPO) as the target enzyme (PDB ID: 1DNU). This study employed molegro virtual docker (MVD) to analyze the docking process, identifying the poses with the best binding energy. Compound **3a** exhibited the highest Moldock score, as shown in Table-4. The protein-ligand interaction results are summarized in Table-5, revealing the common interactions of all the compounds with Ala24 and Thr21. These interactions suggest a potential mode of binding for the bromoanilines with the myeloperoxidase enzyme. These studies allow for the assessment of how the ligand interacts with the active site of the target protein, which is essential for developing effective antioxidant therapies. Fig. 3 illustrates the interaction of compound **3a** at the active site of MPO,

TABLE-3
BDE, IP, PDE, PA AND ETE VALUES OF THE STUDIED COMPOUNDS AS EVALUATED USING THE B3LYP/LANL2DZ LEVEL OF THEORY AND DMSO SOLVENT MEDIUM

Compound	Position	SET-PT		SPLET		HAT
		IP (KJ/mol)	PDE (KJ/mol)	PA (KJ/mol)	ETE (KJ/mol)	BDE (KJ/mol)
1a	C(3)-H	-459.156	-803.851	-940.454	-322.673	-478.366
	C(2)-H		-801.488	-981.149	-279.615	-476.003
	C(1)-H		-802.538	-984.037	-277.777	-477.053
	N-H		-726.406	-1873.031	-687.355	-400.913
2a	C(3)-H	-450.230	-778.649	-945.967	-283.028	-444.234
	C(2)-H		-806.214	-985.875	-270.689	-471.802
	C(1)-H		-809.102	-982.987	-276.465	-474.690
	N-H		-733.494	-1857.278	-673.440	-399.076
3a	C(3)-H	-503.522	-761.847	-941.504	-323.986	-480.729
	C(2)-H		-758.697	-957.257	-305.083	-477.578
	C(1)-H		-763.160	-966.446	-300.357	-482.041
	N-H		-725.881	-1953.372	-723.850	-444.759
4a	C(3)-H	-427.128	-828.528	-996.639	-259.136	-471.014
	C(2)-H		-830.366	-995.327	-262.287	-472.852
	C(1)-H		-831.679	-1016.856	-242.071	-474.165
	N-H		-745.571	-1829.185	-656.375	-388.048
	C(4)-H		-721.418	-1696.073	-547.416	-363.894
5a	C(3)-H	-428.965	829.316	-1021.582	-236.820	-473.640
	C(2)-H		-825.641	-995.327	-259.399	-469.964
	C(1)-H		-832.204	-1018.431	-242.858	-476.528
	N-H		-745.833	-1842.313	-667.402	-390.149
	C(4)-H		-725.881	-1868.043	-713.085	-370.195
6a	C(2)-H	-447.867	-811.202	-986.925	-272.264	-474.427
	C(1)-H		-812.252	-945.180	-315.060	-475.478
	N-H		-730.607	-1845.989	-667.402	-393.825
	C(4)-H		-701.466	-1718.652	-569.208	-364.681
7a	C(2)-H	-420.565	-834.304	-1031.558	-223.430	-470.227
	C(1)-H		-839.554	-1031.033	-229.206	-475.478
	N-H		-744.258	-1813.432	-648.498	-380.172
	C(3)-H		-723.256	-1662.204	-518.273	-359.168
	C(4)-H		-726.406	-1689.509	-542.428	-362.319

TABLE-4
DOCKING SCORE OF THE COMPOUNDS WITH TARGET PDB ID: 1DNU AS PREDICTED BY MVD

Ligand	Moldock score	Rerankscore[a]	Interaction[b]	Internal[c]	Hbond[d]	LE1[e]	LE3[f]
1a	-48.77	-41.05	-55.92	7.15	-3.82	-5.00	-4.37
2a	-46.85	-38.32	-56.34	9.50	-3.76	-5.45	-4.68
3a	-54.98	-48.12	-62.14	7.16	-5.98	-5.42	-4.56
4a	-49.07	-42.14	-56.34	7.26	-3.95	-5.21	-4.26
5a	-50.92	-43.10	-56.65	5.74	-2.96	-5.22	-4.44
6a	-52.19	-44.36	-59.90	7.70	-3.75	-5.11	-3.88
7a	-51.13	-38.83	-58.35	7.22	-3.06	-5.65	-4.79

emphasizing its strong binding affinity and potential therapeutic benefits in reducing oxidative stress. Targeting MPO is particularly relevant for antioxidant studies due to MPO's role in the production of reactive oxygen species (ROS), which contribute to oxidative damage in cells. By effectively binding to MPO, antioxidants can inhibit its activity, thereby reducing ROS production and mitigating oxidative stress. The strong binding affinity of compound **3a** with MPO indicates its potential to interact efficiently with the enzyme, highlighting its capability to reduce ROS production and consequently alleviate oxidative damage.

Analysis of visual molecular dynamics (VMD), non-covalent interaction (NCI) and electron localized function (ELF): The computed interaction energy values for the synthesized compounds with amino acid residues (alanine, threonine and glycine) are presented in Table-6. The sequence of stability for the compound-amino acid complexes is as follows:

For alanine: **7a** < **4a** < **6a** < **5a** < **2a** < **1a** < **3a**

For threonine: **7a** < **5a** ≈ **6a** < **4a** < **2a** < **1a** < **3a**

Quantum mechanical calculations indicate that more negative interaction energy values correlate with greater stab-

TABLE-5
PROTEIN-LIGAND INTERACTION OF THE COMPOUNDS AT THE ACTIVE SITE OF THE TARGET PDB ID:1DNU AS PREDICTED BY MVD

Ligand	Interaction (protein-ligand)	Interaction distance (Å)	Interaction energy (kJ/mol)	Hybridization of protein	Hybridization of ligand
1a	Ala24 (O8)···N(7)	2.92	-2.50	sp^2 (A)	sp^3 (D)
	Thr21 (O8)···N(7)	3.00	-2.50	sp^2 (A)	sp^3 (D)
2a	Ala24 (O8)···N(7)	2.92	-2.50	sp^2 (A)	sp^3 (D)
	Thr21 (O8)···N(7)	3.00	-2.50	sp^2 (A)	sp^3 (D)
3a	Ala24 (O8)···N(7)	2.57	-2.24	sp^2 (A)	sp^3 (D)
	Thr21 (O8)···N(7)	3.13	-2.35	sp^2 (A)	sp^3 (D)
	Gly23 (N7)···N(7)	3.20	-1.98	sp^2 (D)	sp^3 (A)
4a	Ala24 (O8)···N(7)	2.92	-2.50	sp^2 (A)	sp^3 (D)
	Thr21 (O8)···N(7)	3.00	-2.50	sp^2 (A)	sp^3 (D)
5a	Ala24 (O8)···N(7)	3.02	-2.50	sp^2 (A)	sp^3 (D)
	Thr21 (O8)···N(7)	2.60	-2.50	sp^2 (A)	sp^3 (D)
6a	Ala24 (O8)···N(7)	2.92	-2.50	sp^2 (A)	sp^3 (D)
	Thr21 (O8)···N(7)	3.03	-2.50	sp^2 (A)	sp^3 (D)
7a	Ala24 (O8)···N(7)	2.96	-2.50	sp^2 (A)	sp^3 (D)
	Thr21 (O8)···N(7)	2.84	-2.50	sp^2 (A)	sp^3 (D)

A = Acceptor; D = Donor

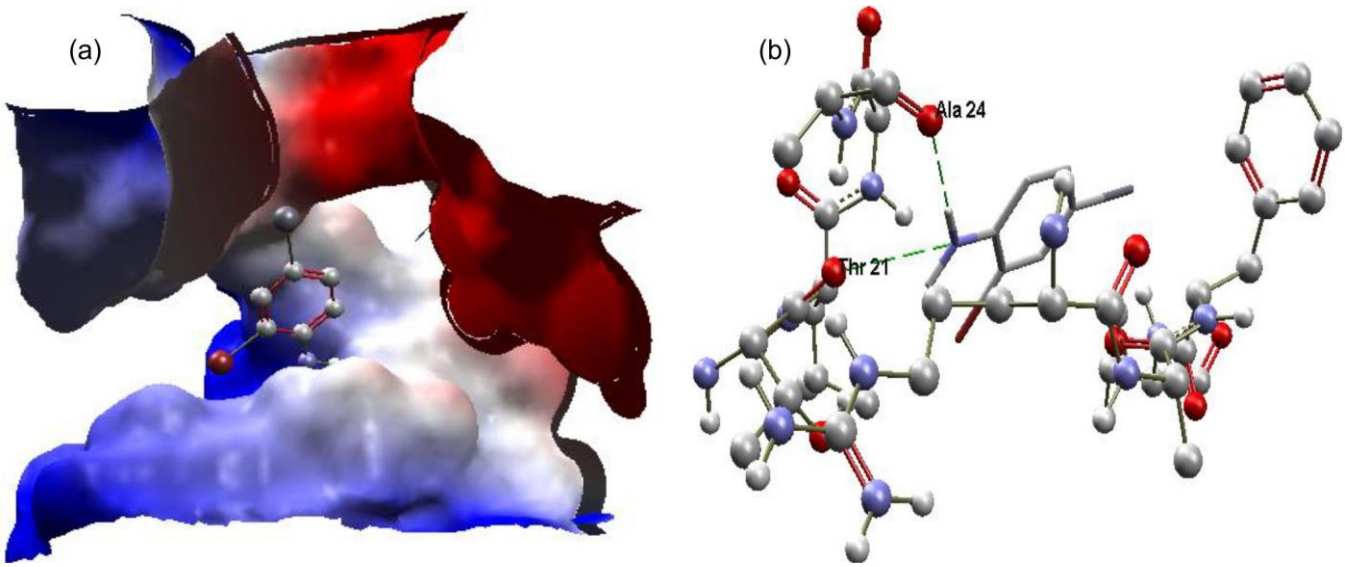

Fig. 3. Compound **3a** (a) at the active pocket of MPO; (b) at the active site of the target PDB ID: 1DNU showing possible mode of interaction

TABLE-6
COMPUTED INTERACTION ENERGIES (kcal/mol) OF THE ANTIOXIDANTS WITH AMINO ACID RESIDUES (PDB ID:1DNU)

Antioxidant agents	Interaction energies (kcal/mol)		
	Alanine	Threonine	Glycine
1a	-18.37	-21.18	–
2a	-17.52	-19.34	–
3a	-27.01	-28.56	–
4a	-14.41	-19.00	–
5a	-16.31	-18.18	–
6a	-14.73	-18.19	–
7a	-13.60	-17.30	–

ility of any complex or dimer [93,94]. It has been observed that lower PA values suggest the SPLET mechanism is more favourable for the studied compounds. This is further supported by the more negative interaction energy values for the compound-amino acid complexes, particularly **3a**, indicating more favourable interactions. In our case, the most favoured **3a**-amino acid complexes exhibit computed interaction energy values of -27.01 kcal/mol for **3a**-alanine and -28.56 kcal/mol for **3a**-threonine. These findings underscore the strong and stable interactions of compound **3a** with these amino acids, further validating the compound's potential efficacy through the SPLET mechanism.

Hence, the study reveals that among all the compounds, **3a**-amino acid complexes exhibit the most negative interaction energy values, with **3a**-alanine and **3a**-threonine found to be -27.01 kcal/mol and -28.56 kcal/mol, respectively. This results in higher stability and a more favoured conformation compared to the other compounds. This enhanced stability is attributed to the formation of strong hydrogen bonds through the $-NH_2$ groups of the amino acid residues. Conversely,

compound **7a** forms the least stable complex with amino acid residues, as indicated by its less negative interaction energy values, as shown in Table-6.

Non-covalent interaction and iso-surface analysis: The NCI scatter diagram provides insights into the preferred interacting sites of a molecular complex, distinguishing between strong and weak directional attractions. By analyzing the spikes that appear at low RDG densities in the NCI plot, the nature of interactions within the complex structure can be inferred. Fig. 4 illustrates the visual representation of the NCI scatter plot, which is plotted using RDG and the sign of the second Hessian Eigenvalue (sin λ2ρ), resulting in a stiletto-heel shape. The sign of λ2ρ describes the strength and nature of chemical bonding, including local bonding characteristics in the complex. In the NCI plot, positive values of λ2ρ indicate repulsive/steric hindrance, negative values suggest hydrogen bonding and values close to zero represent van der Waals interactions. The scatter graph encompasses all types of non-covalent interactions observed in the compound-protein complex system, with weak van der Waals interactions represented by green, steric interactions by red and hydrogen bonding by blue. These weak interactions play a crucial role in drug delivery as they facilitate the release of drugs from therapeutic agents at specific target sites. In this study, van der Waals interactions were found to be more prevalent in both alanine and threonine complexes. For the antioxidant activity of bromoanilines such as **1a**, **3a** and **4a**, the compounds-alanine complex exhibited stronger van der Waals interactions compared to the compounds-threonine complexes. Similarly, in case of **2a**, **5a**, **6a** and **7a**, the compounds-threonine complexes were more predominant than the compounds-alanine complexes. Notably, all the compounds and amino acid complexes displayed highly effective van der Waals interactions, as depicted in the NCI graph shown in Fig. 4.

Visual molecular dynamics analysis: The 3D colour-filled iso-surface of compounds interacting with target proteins was crafted using visual molecular dynamics (VMD), presenting a captivating visual in Fig. 5. In this, vibrant green areas denote weak van der Waals interactions between the antioxidant activity of bromoanilines and alanine/ threonine/ glycine within the target protein. The colour-filled reduced density gradient (RDG) isosurface offers a nuanced view, allowing for the identification of different regions based on their colours. Deep shades of blue signify robust attractive interactions, while a light blue hue indicates the presence of an elliptical slab between oxygen and hydrogen atoms, hinting at the existence of a hydrogen bond, *albeit* not particularly strong. The green circle on the plot signifies the van der Waals interaction region, marked by a green or light brown colour, indicative of low electron density in that area. Regions filled with red denote intense steric interactions, particularly near the centre of the two rings. Delving into the specifics, the VMD plots unveil the precise interacting sites between the compounds and the amino acid residues. These visual representations provide a captivating glimpse into the intricate dance of molecular interactions within the complex, shedding light on the mechanisms underlying antioxidant activity at a molecular level.

Analysis of electron density changes: The electron localization function (ELF) in quantum chemistry serves as a valuable tool for pinpointing electron pairs within specific regions of space. Through ELF analysis, alterations in electron charge density can be scrutinized in both unstacked compounds and their complex formations with alanine, threonine and glycine of the target protein. Fig. 6 illustrates the ELF plots of the studied compounds, offering a visual depiction of their interaction with the target protein. Noticeable shifts in electron density are observed following the formation of complexes with alanine, threonine and glycine. ELF values span from 0.0 to 1.0, with values between 0.5 and 1.0 indicating regions where electrons are localized, occupying both bonding and anti-bonding space. Conversely, regions with delocalized electrons exhibit lower ELF values, ranging from 0.0 to 0.5. Consequently, these ELF plots facilitate the examination of transitions from the compounds to alanine, threonine and glycine, as well as the density alterations in the compounds following complex formation.

The ELF figures for compound **3a** exhibit consistent scale and appearance, indicating uniform ELF values for both the individual and interacted **3a** complexes. This consistency suggests a stable electron distribution, contributing to the overall stability of the compound. Such stability is advantageous in predicting the antioxidant activity of compound. Antioxidants typically function by donating electrons to neutralize free radicals and a stable electron distribution enhances this process efficiency. The uniform ELF values observed across compound **3a** signify a stable electron distribution, facilitating the effective electron transfer and antioxidant activity [95].

Physico-chemical, medicinal and toxicity analysis

Analysis of physico-chemical property: A summary of all the physico-chemical properties was calculated by using ADMETlab [87]. Herein, compound **3a** complies with the Lipinski's rule of five, indicating its potential as an oral drug candidate due to its molecular weight of 215.95 g/mol, with 4 hydrogen bond acceptors (nHA) and 2 hydrogen bond donors, along with only 1 rotatable bond, hence it is suitable for oral drug development (Table-7). Compound **3a** does not carry a formal charge, falling within the ideal range for drug candidates between -4 to 4. Its topological polar surface area (TPSA) is 69.16 $Å^2$ within a range of 0-140 $Å^2$. The aqueous solubility (log S) of compound **3a** is -3.32, within the optimal range of -4 to 0.5 log mol/L. The partition coefficient (log P) value, representing the octanol/water partition coefficient, is 2.45, indicating partitioning into the lipid compartment. At a normal physiological pH of 7.4, the log D or partition coefficient is 2.21, falling within the optimal range of 1 to 3.

Again, SwissADME also helps for analyzing radar chart displaying oral bioavailability of the compounds as depicted in Fig. 7 [96]. Fig. 8 represents a radar chart illustrating the physico-chemical properties of the compounds, where all characteristics of the most favoured compound **3a** fall within the acceptable upper and lower limits, except for the log P and log D values of antioxidants **1a**, **2a** and **6a**.

Analysis of medicinal properties: Table-8 outlines the details of medicinal properties for all the compounds under study. Compound **3a** has a QED score of 0.44, falling below

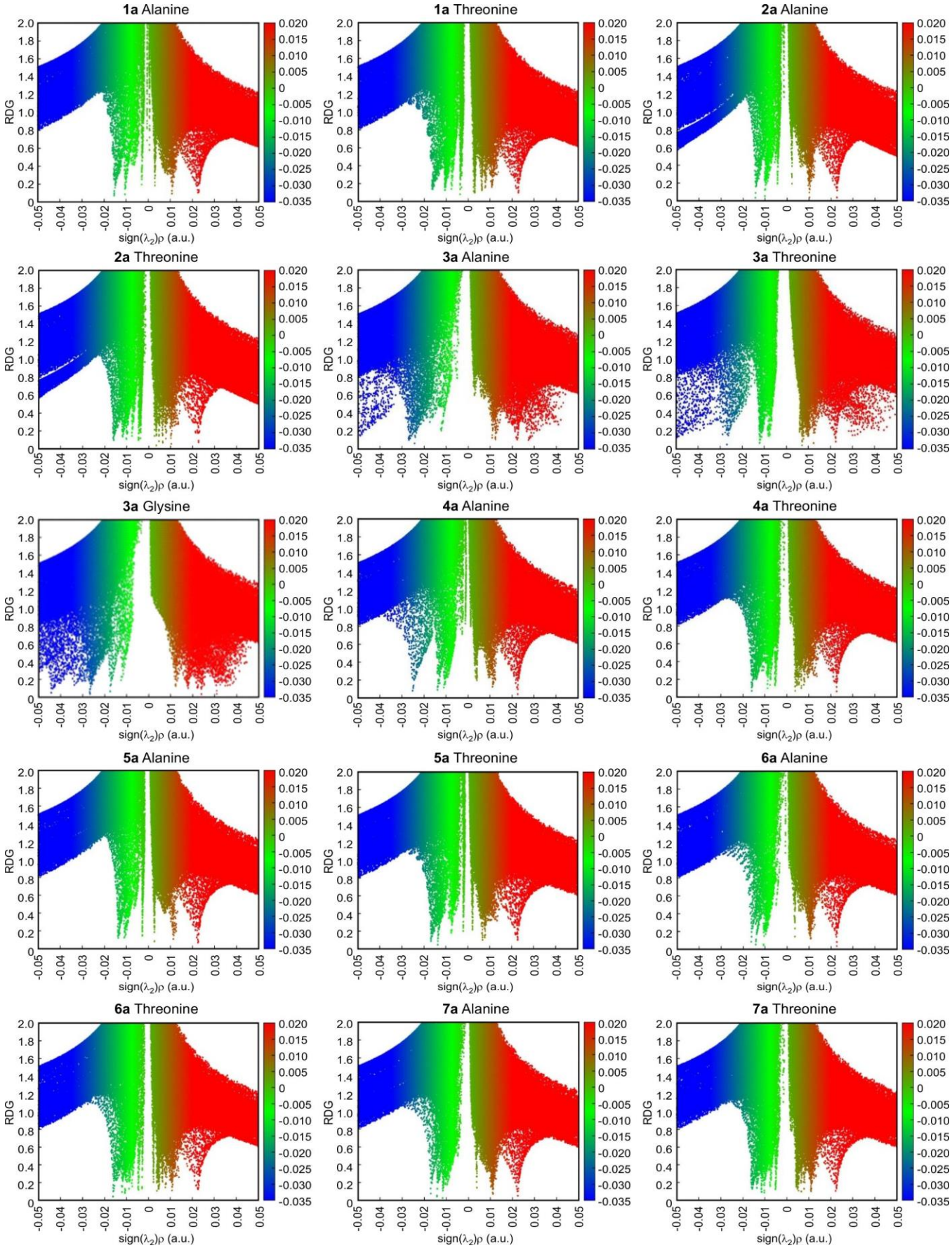

Fig. 4. NCI diagram of compounds **1a-7a** with alanine, threonine and glycine

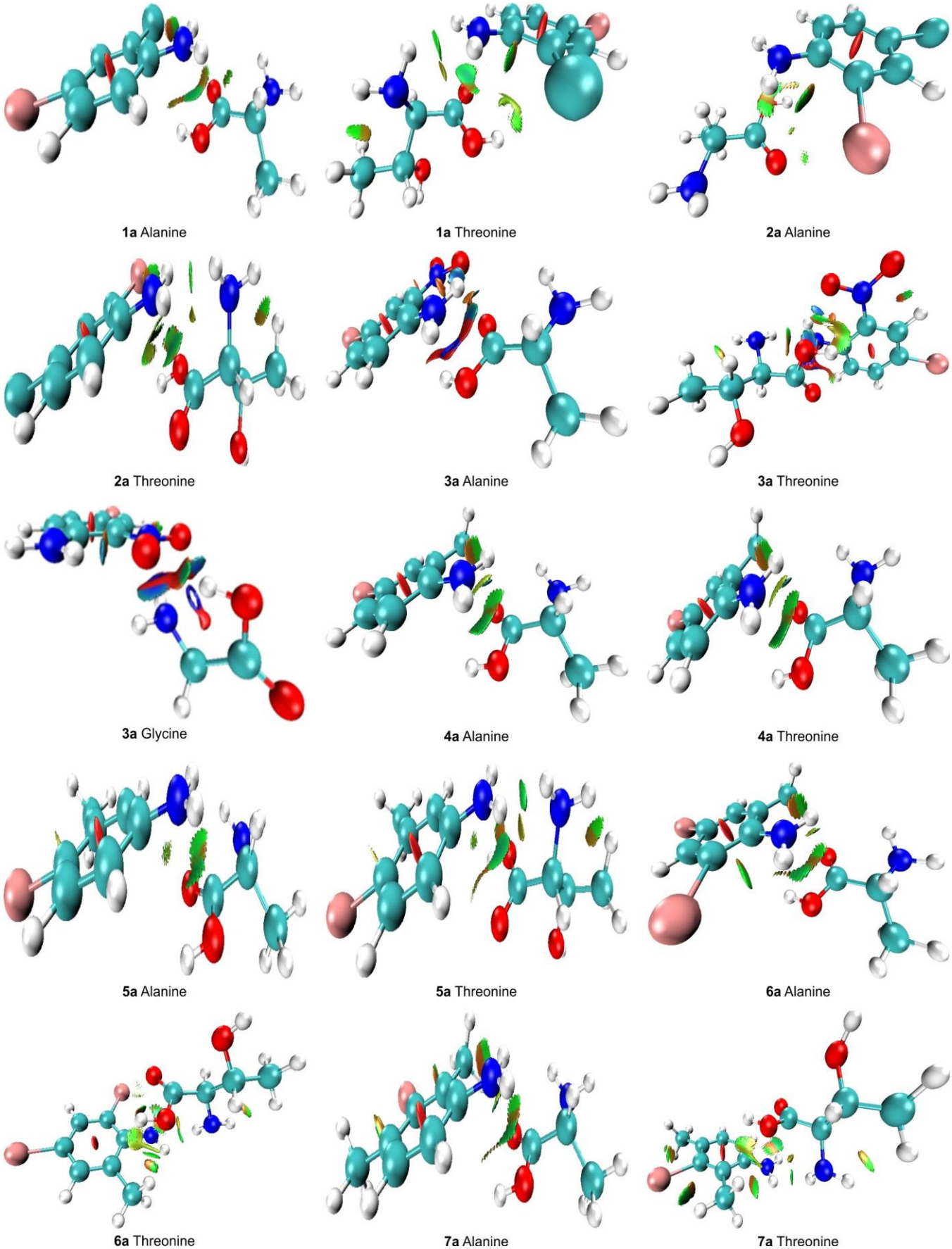

Fig. 5. VMD analysis for the most favoured antioxidant-**1a-7a** with alanine, threonine and glycine residues

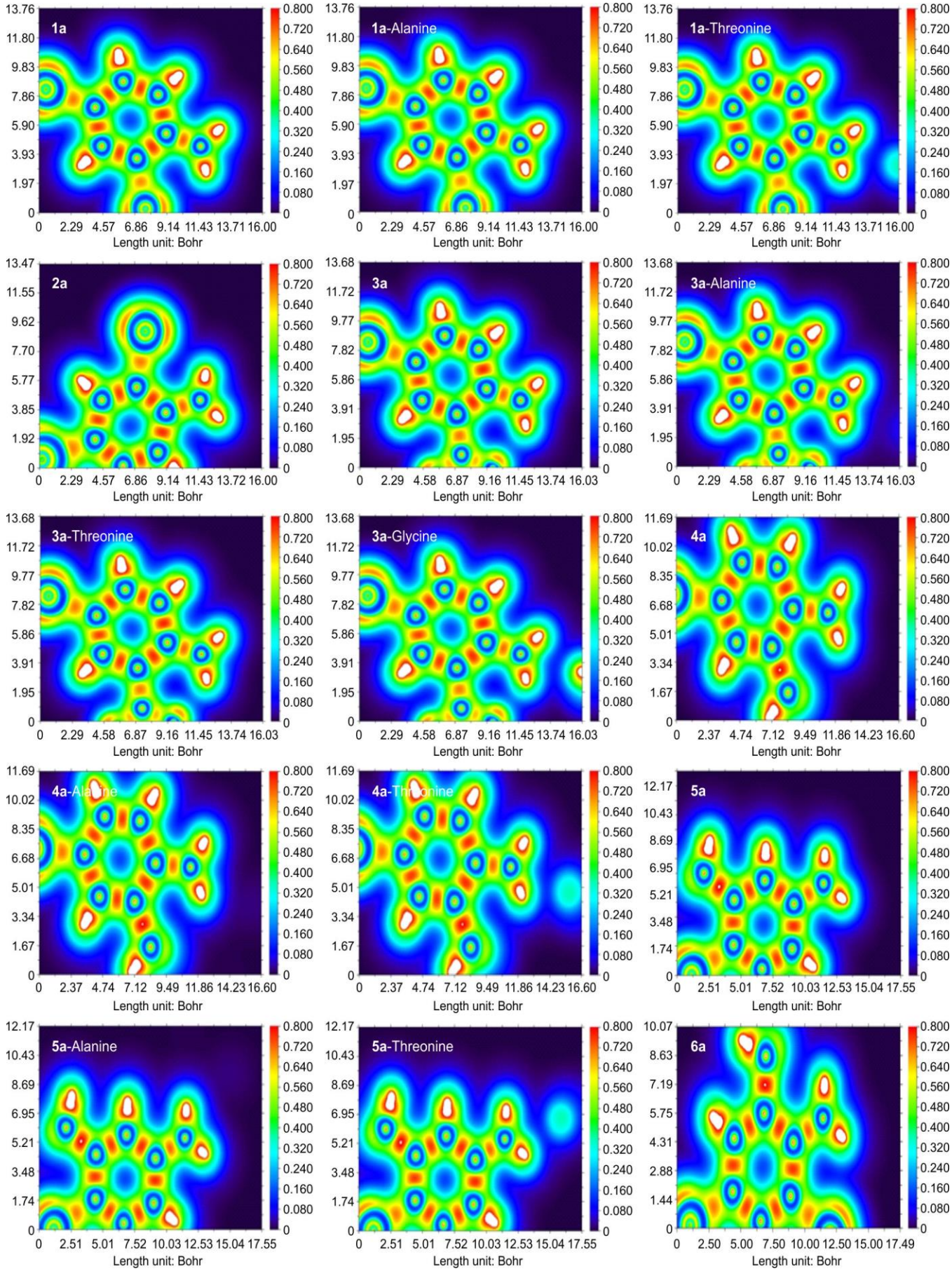
1a
1a-Alanine
1a-Threonine
2a
3a
3a-Alanine
3a-Threonine
3a-Glycine
4a
4a-Alanine
4a-Threonine
5a
5a-Alanine
5a-Threonine
6a
Length unit: Bohr

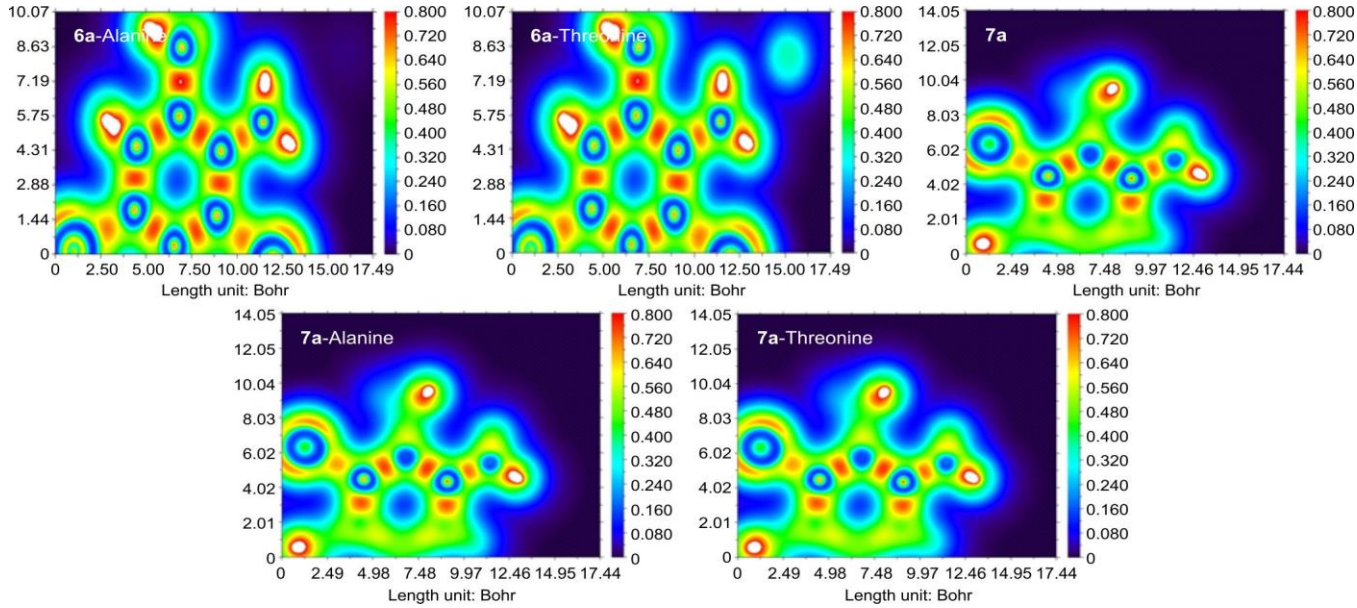

Fig. 6. ELF diagrams of compound **1a-7a** (individual) with alanine, threonine and glycine

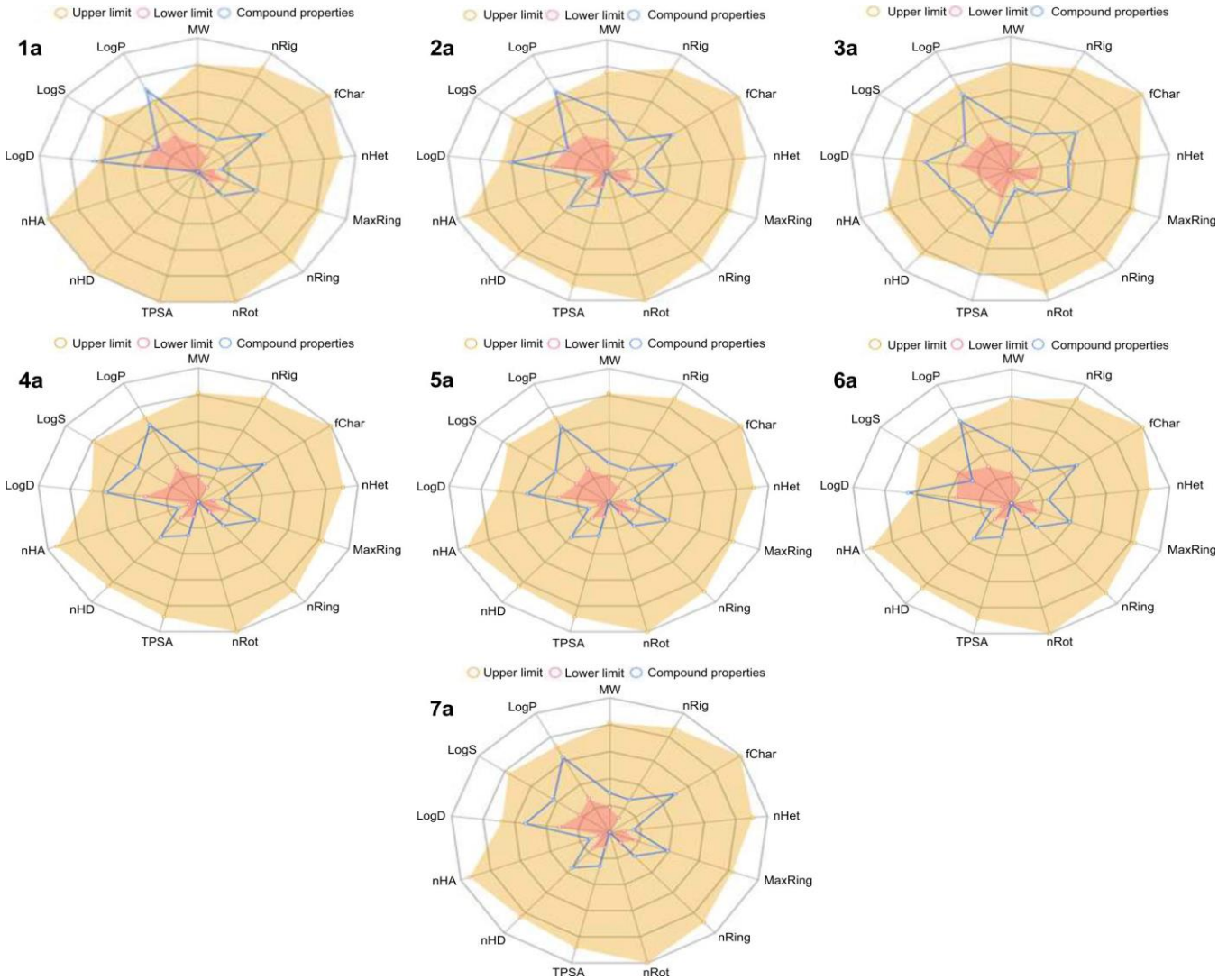

Fig. 7. Physico-chemical properties radar chart for **1a**, **2a**, **3a**, **4a**, **5a**, **6a** and **7a**. Brownish regions define the upper limit, pinkish region defines the lower limit and bluish lines represent the compound parameters (ADMETlab 2.0)

TABLE-7
PHYSICO-CHEMICAL PROPERTIES ANALYSIS OF ANTIOXIDANT COMPOUND

Compound	MW (g/mol)	nHA	nHD	TPSA	MR	nRot	fChar	logS	log P	logD
1a	203.93	0	0	0	44.12	0	0	-4.35	4.14	3.21
2a	296.87	1	2	26.02	51.26	0	0	-4.23	3.34	2.65
3a	215.95	4	2	69.16	47.37	1	0	-3.32	2.45	2.21
4a	184.98	1	2	26.02	43.51	0	0	-2.07	2.54	2.45
5a	184.98	1	2	26.02	43.51	0	0	-2.62	2.47	2.05
6a	262.89	1	2	26.02	51.21	0	0	-5.68	3.04	3.32
7a	184.98	1	2	26.02	43.51	0	0	-2.36	2.38	2.19

*Hydrogen bond acceptors (nHA) and donors (nHD), rotatable bonds (nRot), formal charge (fChar), topological polar surface area (TPSA), molar refractivity (MR), aqueous solubility (logS), partition coefficient (log P), its value at physiological pH (logD).

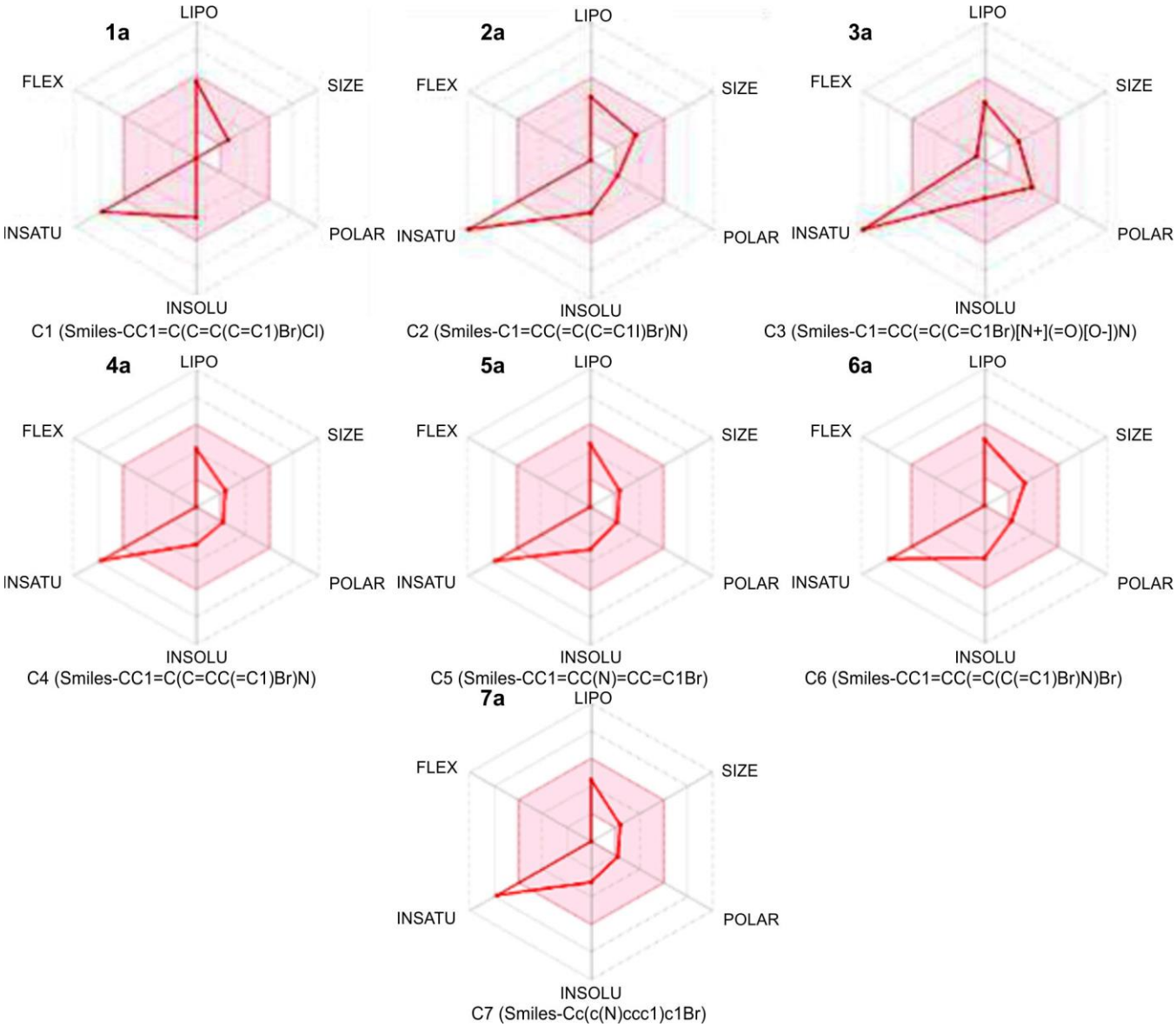

Fig. 8. Oral bioavailability radar chart for **1a**, **2a**, **3a**, **4a**, **5a**, **6a** and **7a**

the ideal threshold value of 0.67. Fraction of sp^3 hybridization (Fsp^3) values for all antioxidants are 0.14, indicating non-compliance with the acceptable threshold of 0.42 except for **2a** and **3a** (Table-8). The medicinal chemistry evaluation, MCE-18 scores for all compounds are below the optimal limit of ≥ 45; all compounds adhere to Lipinski's rule parameters: MW ≤ 500, log P ≤ 5, Hacc ≤ 10, Hdon ≤ 5. However, they fail to satisfy the Pfizer rule (log P > 3 and TPSA < 75 Å^2) and the GSK rule of drug-likeness. Nonetheless, they meet the criteria outlined in the Golden Triangle rule. PAINS alerts are absent in all compounds, ensuring exclusion from lists of frequent hitters and reactive compounds.

TABLE-8
MEDICINAL CHEMISTRY ANALYSIS OF ANTIOXIDANT COMPOUND

Compound	QED	Fsp^3	MCE-18	Lipinski rule	Pfizer rule	Gsk rule	Golden triangle rule	PAINS	AlARM NMR	Chealator rule
1a	0.61	0.14	6	Accepted	Rejected	Rejected	Accepted	0	1	0
2a	0.58	0	6	Accepted	Rejected	Accepted	Accepted	0	2	0
3a	0.44	0	7	Accepted	Accepted	Accepted	Accepted	0	3	0
4a	0.62	0.14	6	Accepted	Accepted	Accepted	Rejected	0	2	0
5a	0.62	0.14	6	Accepted	Accepted	Accepted	Rejected	0	2	0
6a	0.72	0.14	7	Accepted	Rejected	Accepted	Accepted	0	2	0
7a	0.62	0.14	6	Accepted	Accepted	Accepted	Rejected	0	2	0

*Quantitative estimate drug-likeness (QED), the fraction of sp^3 hybridized carbons (Fsp^3), medicinal chemistry evolution (MCE-18) and potential interference with assays (PAINS).

Toxicity analysis: Table-9 displays the toxicity parameters projected by "predhERG", encompassing factors such as hERG cardiotoxicity and the potency of the compounds [97]. Results from the dedicated web server, "predhERG", consistently evaluated all compounds for hERG cardiotoxicity. According to the predhERG web server, none of the compounds were predicted to have hERG cardiotoxicity, all compounds being identified as non-blockers with a high average confidence of 97.01%. Specifically, compound **3a** was identified as a weak blocker, while the other compounds were categorized as moderate blockers with a lower average confidence of 39.38%.

By comparing the theoretical IC_{50} value of the studied compounds with known antioxidants to contextualize its efficacy. The calculated IC_{50} value of the antioxidant **3a** is found to be 5.11 µM by using the Pred-heRG web tool, which indicates the concentration at which the complex inhibits 50% of its target, providing a quantitative measure of its potency. To demonstrate that the synthesized compounds is an effective antioxidant, we undertook a comprehensive approach combining theoretical calculations and experimental validation. In present case, antioxidant-**3a** exhibits experimental IC_{50} value is found to be 5.77 µM (*i.e.* 1.73 ± 0.3 mg/mL), which has structural features conducive to antioxidant activity, including four hydrogen bond acceptors and two hydrogen bond donors; thus, it demonstrates a high level of potency, referring as a favourable among well-established antioxidants.

Conclusion

The present work was carried out to look more into the intrinsic properties of simple molecules. Bromoanilines synthesized through an environmentally benign pathway were studied for their antioxidant activity. The antioxidant property of the synthesized compounds was determined using DPPH and FRAP assays. While all the compounds showed antioxidant activity, 4-bromo-2-nitroaniline (**3a**) significantly was observed to act as better antioxidants in both radical scavenging and reducing power assay. These results suggest that electron-withdrawing groups, enhance antioxidant activity. Compound **3a**, in molecular docking studies also showed the best MolDock score with the target protein (MPO) which suggests that it has the potential to interact effectively with the enzyme, thereby reducing the production of ROS and mitigating oxidative damage. DFT was employed to study the mechanistic behaviour of the antioxidant activity by analyzing the BDE, PDE, IP, PA and ETE of the studied compounds. The study indicated that SPLET mechanism might be favoured for the antioxidant activity of the studied compounds in the DMSO solvent and the amine group present in the compounds might be responsible for the SPLET mechanism of antioxidant activity. Electron withdrawing groups reduce the proton affinity of the antioxidant molecule, making it easier for the molecule to lose a proton. Additionally, based on the findings from quantum chemical density functional theory (DFT), most of the investigated compounds exhibited effective interactions with amino acids, resulting in negative interaction energy values. However, compound **3a**, displayed a highly favourable interaction with alanine, threonine and glycine, as evidenced by its significantly more negative interaction energy value of -28.56 kcal/mol compared to the other compounds. The computational interaction energy calculations were corroborated by visualizing the favoured model using VMD, NCI and ELF analysis. The diagrams depicting the **3a**-amino acid stacked molecular system clearly demonstrated changes in electron charge densities, mode of interaction and preferred interacting sites. Further the physico-

TABLE-9
PREDICTED Pred-HerG TOXICITY FOR BROMOANILINES

Compounds	Prediction	Confiability (%)	Applicability domain	Categorical potency	Confiability (%)	Applicability domain	Potency	Applicability domain
1a	Non-blocker	94.90	Inside	Moderate blocker	51	Inside	5.26	Inside
2a	Non-blocker	96.97	Outside	Moderate blocker	36.8	Outside	5.22	Outside
3a	Non-blocker	91.68	Outside	Weak blocker	34.26	Outside	5.11	Outside
4a	Non-blocker	99.21	Inside	Moderate blocker	38.24	Inside	5.07	Inside
5a	Non-blocker	99.71	Outside	Moderate blocker	43.21	Outside	5.03	Inside
6a	Non-blocker	97.41	Outside	Moderate blocker	34.11	Outside	5.12	Outside
7a	Non-blocker	99.16	Inside	Moderate blocker	38.02	Inside	4.962	Inside

chemical, medicinal and toxicity parameters screening exhibited favourable outcomes enhancing the understanding of the inherent antioxidant activity of bromoanilines. To validate the therapeutic potential of these compounds, further investingations including *in vivo* studies and clinical trials are essential.

ACKNOWLEDGEMENTS

The author Naruti Longkumer is thankful to NFST fellowship (201819-NFST-NAG-00172); author Rituparna Karmaker is grateful to the DST INSPIRE Fellowship (No. DST/INSPIRE Fellowship/2016/IF160719); author Basanta Singha is thankful for UGC Non-NET fellowship (NU/RDC/NNF-126/2021-3509). The authors also thank DBT Project BT/PR28873/NER/95/1527/2020 for financial assistance.

CONFLICT OF INTEREST

The authors declare that there is no conflict of interests regarding the publication of this article.

REFERENCES

1. M. Antolovich, P.D. Prenzler, E. Patsalides, S. McDonald and K. Robards, *Analyst*, **127**, 183 (2002); https://doi.org/10.1039/b009171p
2. E. Menteşe, F. Yılmaz, N. Baltaş, O. Bekircan and B. Kahveci, *J. Enzyme Inhib. Med. Chem.*, **30**, 435 (2015); https://doi.org/10.3109/14756366.2014.943203
3. Y. Dong, T.K. Venkatachalam, R.K. Narla, V.N. Trieu, E.A. Sudbeck and F.M. Uckun, *Bioorg. Med. Chem. Lett.*, **10**, 87 (2000); https://doi.org/10.1016/S0960-894X(99)00581-8
4. N. Mihailović, V. Marković, I.Z. Matić, N.S. Stanisavljević, Ž.S. Jovanović, S. Trifunović and L. Joksović, *RSC Adv.*, **7**, 8550 (2017); https://doi.org/10.1039/C6RA28787E
5. E. Bendary, R.R. Francis, H.M.G. Ali, M.I. Sarwat and S. El Hady, *Ann. Agric. Sci.*, **58**, 173 (2013); https://doi.org/10.1016/j.aoas.2013.07.002
6. S.K. Madhusudan and A.K. Misra, *Carbohydr. Res.*, **340**, 497 (2005); https://doi.org/10.1016/j.carres.2004.12.002
7. E. Tayama, R. Sato, K. Takedachi, H. Iwamoto and E. Hasegawa, *Tetrahedron*, **68**, 4710 (2012); https://doi.org/10.1016/j.tet.2012.04.015
8. E.D. Matveeva, T.A. Podrugina and N.S. Zefirov, *Mendeleev Commun.*, **8**, 21 (1998); https://doi.org/10.1070/MC1998v008n01ABEH000729
9. J.D. Pelletier and D. Poirier, *Tetrahedron Lett.*, **35**, 1051 (1994); https://doi.org/10.1016/S0040-4039(00)79963-1
10. Q. Zhou, Y. Bao and G. Yan, *Adv. Synth. Catal.*, **364**, 1371 (2022); https://doi.org/10.1002/adsc.202200023
11. A. Ruíz-Baltazar, *Int. Res. J. Pure Appl. Chem.*, **4**, 263 (2014); https://doi.org/10.9734/IRJPAC/2014/7595
12. M.B. Floyd, M.T. Du, P.F. Fabio, L.A. Jacob and B.D. Johnson, *J. Org. Chem.*, **50**, 5022 (1985); https://doi.org/10.1021/jo00225a004
13. S. Ghammamy, K. Mehrani, H. Afrand, Z. Javanshir, G. Rezaeibéhbahani, A. Moghimi and Z.S. Aghbolagh, *J. Chil. Chem. Soc.*, **54**, (2009); https://doi.org/10.4067/S0717-97072009000400038
14. A.K. Singh, V. Singh, S. Rahmani, B. Singh and B. Singh, *J. Mol. Catal. Chem.*, **197**, 91 (2003); https://doi.org/10.1016/S1381-1169(02)00590-3
15. K. Murai, T. Matsushita, A. Nakamura, S. Fukushima, M. Shimura and H. Fujioka, *Angew. Chem. Int. Ed.*, **49**, 9174 (2010); https://doi.org/10.1002/anie.201005409
16. C.H. Cook and E.K. Kang, *Arch. Pharm. Res.*, **4**, 137 (1981); https://doi.org/10.1007/BF02855758
17. C.H. Cook and Y.S. Chung, *Arch. Pharm. Res.*, **4**, 133 (1981); https://doi.org/10.1007/BF02855757
18. G. Gopalakrishnan, V. Kasinath, N.D. Pradeep Singh, V.P. Santhana Krishnan, K.A. Solomon and S.S. Rajan, *Molecules*, **7**, 412 (2002); https://doi.org/10.3390/70500412
19. M. Murai, R. Hatano, S. Kitabata and K. Ohe, *Chem. Commun.*, **47**, 2375 (2011); https://doi.org/10.1039/C0CC04385K
20. D. Urankar, I. Rutar, B. Modec and D. Dolenc, *Eur. J. Org. Chem.*, **2005**, 2349 (2005); https://doi.org/10.1002/ejoc.200400829
21. J.J. Xia, X.L. Wu and G.W. Wang, *ARKIVOC*, **2008**, 22 (2008); https://doi.org/10.3998/ark.5550190.0009.g03
22. A.J. Borah and P. Phukan, *Tetrahedron Lett.*, **53**, 3035 (2012); https://doi.org/10.1016/j.tetlet.2012.04.011
23. D.K. Yadav, A.K. Yadav, V.P. Srivastava, G. Watal and L.D.S. Yadav, *Tetrahedron Lett.*, **53**, 2890 (2012); https://doi.org/10.1016/j.tetlet.2012.03.129
24. K. Richa, R. Karmaker, N. Longkumer, V. Das, P.J. Bhuyan, M. Pal and U.B. Sinha, *Anticancer. Agents Med. Chem.*, **19**, 2211 (2020); https://doi.org/10.2174/1871520619666190930122137
25. S.C. Jeyaseelan, A.M.F. Benial and K. Kaviyarasu, *J. Mol. Recognit.*, **34**, (2020); https://doi.org/10.1002/jmr.2873
26. M. Chaudhary, N. Kumar, A. Baldi, R. Chandra, M.A. Babu and J. Madan, *J. Biomol. Struct. Dyn.*, **38**, 1335 (2020); https://doi.org/10.1080/07391102.2019.1604266
27. É.A. Enyedy, G.M. Bognár, N.V. Nagy, T. Jakusch, T. Kiss and D. Gambino, *Polyhedron*, **67**, 242 (2014); https://doi.org/10.1016/j.poly.2013.08.053
28. A.S. Berezin, *J. Mol. Struct.*, **1336**, 142110 (2025); https://doi.org/10.1016/j.molstruc.2025.142110
29. K.S. Patel, J.C. Patel, H.R. Dholariya and K.D. Patel, *Spectrochim. Acta A Mol. Biomol. Spectrosc.*, **96**, 468 (2012); https://doi.org/10.1016/j.saa.2012.05.057
30. B. Jadou, A. Hameed and A. Al-Rubaie, *Egypt. J. Chem.*, **0**, 0 (2020); https://doi.org/10.21608/ejchem.2020.43195.2872
31. D.G. Ivanchenko, N.I. Romanenko and V.I. Kornienko, *Chem. Nat. Compd.*, **54**, 532 (2018); https://doi.org/10.1007/s10600-018-2397-9
32. N. Longkumer, K. Richa, R. Karmaker, V. Kuotsu, A. Supong, L. Jamir, P. Bharali and U. Bora Sinha, *Acta Chim. Slov.*, **66**, 276 (2019); https://doi.org/10.17344/acsi.2018.4580
33. K. Iwasa, D.U. Lee, S.I. Kang and W. Wiegrebe, *J. Nat. Prod.*, **61**, 1150 (1998); https://doi.org/10.1021/np980044+
34. H. Vural and M. Kara, *Optik*, **145**, 479 (2017); https://doi.org/10.1016/j.ijleo.2017.08.032
35. V.K. Bhovi, Y.D. Bodke, S. Biradar, B.E.K. Swamy and S. Umesh, *Phosphorus Sulfur Silicon Relat. Elem.*, **185**, 110 (2009); https://doi.org/10.1080/10426500902717317
36. G.S. Fasiuddin, F.L.A. Khan, S. Sakthivel, S. Muthu and A. Irfan, *J. Mol. Struct.*, **1261**, 132815 (2022); https://doi.org/10.1016/j.molstruc.2022.132815
37. R.V. Kusurkar, R.H. Rayani, D.R. Parmar, M.N. Bhoi, V.H. Zunjar and J.Y. Soni, *Results Chem.*, **4**, 100357 (2022); https://doi.org/10.1016/j.rechem.2022.100357
38. W. Zhao, X. Feng, S. Ban, W. Lin and Q. Li, *Bioorg. Med. Chem. Lett.*, **20**, 4132 (2010); https://doi.org/10.1016/j.bmcl.2010.05.068
39. H. Wang, K. Wen, N. Nurahmat, Y. Shao, H. Zhang, C. Wei, Y. Li, Y. Shen and Z. Sun, *Beilstein J. Org. Chem.*, **8**, 744 (2012); https://doi.org/10.3762/bjoc.8.84
40. S.P. Borikar, T. Daniel and V. Paul, *Tetrahedron Lett.*, **50**, 1007 (2009); https://doi.org/10.1016/j.tetlet.2008.12.053
41. B. Das, K. Venkateswarlu, A. Majhi, V. Siddaiah and K.R. Reddy, *J. Mol. Catal. Chem.*, **267**, 30 (2007); https://doi.org/10.1016/j.molcata.2006.11.002
42. P.V. Ghorpade, D.A. Pethsangave, S. Some and G.S. Shankarling, *J. Org. Chem.*, **83**, 7388 (2018); https://doi.org/10.1021/acs.joc.8b00188
43. H. Tajik, I. Mohammadpoor-Baltork, P. Hassan-Zadeh and H.R. Rashtabadi, *Russ. J. Org. Chem.*, **43**, 1282 (2007); https://doi.org/10.1134/S1070428007090047
44. Y.K. Al-Majedy, D.L. Al-Duhaidahawi, K.F. Al-Azawi, A.A. Al-Amiery, A.A.H. Kadhum and A.B. Mohamad, *Molecules*, **21**, 135 (2016); https://doi.org/10.3390/molecules21020135
45. D. Lahiri, S. Dash, R. Dutta and M. Nag, *J. Biosci.*, **44**, 52 (2019); https://doi.org/10.1007/s12038-019-9868-4

46. K. Ecevit, A.A. Barros, J.M. Silva and R.L. Reis, *Future Pharmacol.*, **2**, 460 (2022); https://doi.org/10.3390/futurepharmacol2040030
47. M. Sathiya Deepika, R. Thangam, P. Sakthidhasan, S. Arun, S. Sivasubramanian and R. Thirumurugan, *Food Control*, **90**, 282 (2018); https://doi.org/10.1016/j.foodcont.2018.02.044
48. W. Lee and D.G. Lee, *Biochem. Biophys. Res. Commun.*, **489**, 228 (2017); https://doi.org/10.1016/j.bbrc.2017.05.138
49. S.C. Yang, C.H. Tseng, P.W. Wang, P.L. Lu, Y.H. Weng, F.L. Yen and J.Y. Fang, *Front. Microbiol.*, **8**, 1103 (2017); https://doi.org/10.3389/fmicb.2017.01103
50. X. Ren, P. An, X. Zhai, S. Wang and Q. Kong, *Lebensm. Wiss. Technol.*, **101**, 100 (2019); https://doi.org/10.1016/j.lwt.2018.11.038
51. D.K. Joung, S.H. Mun, S.H. Choi, O.H. Kang, S.B. Kim, Y.S. Lee, T. Zhou, R. Kong, J.G. Choi, D.W. Shin, Y.C. Kim, D.S. Lee and D.Y. Kwon, *Exp. Ther. Med.*, **12**, 1579 (2016); https://doi.org/10.3892/etm.2016.3486
52. D. Singh, R. Mendonsa, M. Koli, M. Subramanian and S.K. Nayak, *Toxicol. Appl. Pharmacol.*, **367**, 23 (2019); https://doi.org/10.1016/j.taap.2019.01.025
53. F. Bakkali, S. Averbeck, D. Averbeck and M. Idaomar, *Food Chem. Toxicol.*, **46**, 446 (2008); https://doi.org/10.1016/j.fct.2007.09.106
54. P.M.S. Sahoo, S. Behera, R. Behura, A. Acharya, D. Biswal, S.K. Suna, R. Sahoo, R.C. Soren and B.R. Jali, *Biointerface Res. Appl. Chem.*, **12**, 3247 (2021); https://doi.org/10.33263/BRIAC123.32473258
55. O. Inanami, T. Yamamori, H. Shionoya and M. Kuwabara, eds.: H. Sawada, H. Yokosawa and C.C. Lambert, Antioxidant Activity of Quinone-derivatives from Freeze-dried Powder of the Ascidians. In: The Biology of Ascidians. Springer, Tokyo, pp. 457–462 (2001).
56. S. Debnath, A. Agarwal, N.R. Kumar and A. Bedi, *Future Pharmacol.*, **2**, 595 (2022); https://doi.org/10.3390/futurepharmacol2040036
57. A.A. Al-Amiery, *Res. Chem. Intermed.*, **38**, 745 (2012); https://doi.org/10.1007/s11164-011-0414-8
58. A.A. Almehizia, H.A. Abuelizz, H.A.A. Taie, A. ElHassane, M. Marzouk and R. Al-Salahi, *Saudi Pharm. J.*, **27**, 133 (2019); https://doi.org/10.1016/j.jsps.2018.09.006
59. H. Cao, W.X. Cheng, C. Li, X.L. Pan, X.G. Xie and T.H. Li, *J. Mol. Struct. THEOCHEM*, **719**, 177 (2005); https://doi.org/10.1016/j.theochem.2005.01.029
60. M. Reis, B. Lobato, J. Lameira, A.S. Santos and C.N. Alves, *Eur. J. Med. Chem.*, **42**, 440 (2007); https://doi.org/10.1016/j.ejmech.2006.11.008
61. N.F. Santos-Sánchez, R. Salas-Coronado, C. Villanueva-Cañongo and B. Hernández-Carlos, in eds.: E. Shalaby, Antioxidant Compounds and Their Antioxidant Mechanism, IntechOpen eBooks (2019).
62. N. Zhang, Y. Wu, M. Qiao, W. Yuan, X. Li, X. Wang, J. Sheng and C. Zi, *Struct. Chem.*, **33**, 795 (2022); https://doi.org/10.1007/s11224-022-01895-2
63. K. Richa, R. Karmaker, T. Ao, N. Longkumer, B. Singha and U.B. Sinha, *Chem. Phys. Lett.*, **753**, 137611 (2020); https://doi.org/10.1016/j.cplett.2020.137611
64. B. Singha, B. Arora, R. Karmaker, K. Richa, N. Longkumer, M. Abid, H.T. Abdulhameed and U.B. Sinha, *ChemistrySelect*, **9**, e202304761 (2024); https://doi.org/10.1002/slct.202304761
65. M. Gupta, R. Sharma and A. Kumar, *Comput. Biol. Chem.*, **76**, 210 (2018); https://doi.org/10.1016/j.compbiolchem.2018.06.005
66. B. Chami, N.J.J. Martin, J.M. Dennis and P.K. Witting, *Arch. Biochem. Biophys.*, **645**, 61 (2018); https://doi.org/10.1016/j.abb.2018.03.012
67. Y. Aratani, *Arch. Biochem. Biophys.*, **640**, 47 (2018); https://doi.org/10.1016/j.abb.2018.01.004
68. P.T. Goud, D. Bai and H.M. Abu-Soud, *Int. J. Biol. Sci.*, **17**, 62 (2021); https://doi.org/10.7150/ijbs.51811
69. B.S. Chethan and N.K. Lokanath, *J. Mol. Struct.*, **1251**, 131936 (2022); https://doi.org/10.1016/j.molstruc.2021.131936
70. N.S. Venkataramanan and A. Suvitha, *J. Mol. Graph. Model.*, **81**, 50 (2018); https://doi.org/10.1016/j.jmgm.2018.02.010
71. W. Humphrey, A. Dalke and K. Schulten, *J. Mol. Graph.*, **14**, 33 (1996); https://doi.org/10.1016/0263-7855(96)00018-5
72. T. Lu and F. Chen, *J. Comput. Chem.*, **33**, 580 (2012); https://doi.org/10.1002/jcc.22885
73. J. Yana, N. Chiangraeng, P. Nimmanpipug and V.S. Lee, *J. Mol. Graph. Model.*, **107**, 107946 (2021); https://doi.org/10.1016/j.jmgm.2021.107946
74. M. Oyaizu, *Eiyogaku Zasshi*, **44**, 307 (1986); https://doi.org/10.5264/eiyogakuzashi.44.307
75. M.J. Frisch, G.W. Trucks, H.B. Schlegel, G.E. Scuseria, M.A. Robb, J.R. Cheeseman, G. Scalmani, V. Barone, B. Mennucci, G.A. Petersson, H. Nakatsuji, M. Caricato, X. Li, H.P. Hratchian, A.F. Izmaylov, J. Bloino, G. Zheng, J.L. Sonnenberg, M. Hada, M. Ehara, K. Toyota, R. Fukuda, J. Hasegawa, M. Ishida, T. Nakajima, Y. Honda, O. Kitao, H. Nakai, T. Vreven, J.A. Montgomery, Jr., J.E. Peralta, F. Ogliaro, M. Bearpark, J.J. Heyd, E. Brothers, K.N. Kudin, V.N. Staroverov, R. Kobayashi, J. Normand, K. Raghavachari, A. Rendell, J.C. Burant, S.S. Iyengar, J. Tomasi, M. Cossi, N. Rega, J.M. Millam, M. Klene, J.E. Knox, J.B. Cross, V. Bakken, C. Adamo, J. Jaramillo, R. Gomperts, O. Yazyev, R.E. Stratmann, A.J. Austin, R. Cammi, C. Pomelli, J.W. Ochterski, R.L. Martin, K. Morokuma, V.G. Zakrzewski, P. Salvador, G.A. Voth, J.J. Dannenberg, S. Dapprich, A.D. Daniels, O. Farkas, J.B. Foresman, J.V. Ortiz, J. Cioslowski and D.J. Fox, Gaussian 09, Revision A.02, Gaussian, Inc., Wallingford CT (2009).
76. R.D. Vargas-Sánchez, A.M. Mendoza-Wilson, R.R. Balandrán-Quintana, G.R. Torrescano-Urrutia and A. Sánchez-Escalante, *Comput. Theor. Chem.*, **1058**, 21 (2015); https://doi.org/10.1016/j.comptc.2015.01.014
77. R. Karmaker, N.B. Kuotsu, A. Ganguly, N. Guchhait and U.B. Sinha, *Chem. Phys. Lett.*, **711**, 118 (2018); https://doi.org/10.1016/j.cplett.2018.09.022
78. P. Škorňa, J. Rimarčík and E. Klein, *Acta Chim. Slov.*, **7**, 31 (2014); https://doi.org/10.2478/acs-2014-0006
79. G. Wang, Y. Xue, L. An, Y. Zheng, Y. Dou, L. Zhang and Y. Liu, *Food Chem.*, **171**, 89 (2015); https://doi.org/10.1016/j.foodchem.2014.08.106
80. S.J. Blanksby and G.B. Ellison, *Acc. Chem. Res.*, **36**, 255 (2003); https://doi.org/10.1021/ar020230d
81. G. Mazzone, N. Malaj, A. Galano, N. Russo and M. Toscano, *RSC Adv.*, **5**, 565 (2015); https://doi.org/10.1039/C4RA11733F
82. A. Galano, M. Francisco-Márquez and J.R. Alvarez-Idaboy, *Phys. Chem. Chem. Phys.*, **13**, 11199 (2011); https://doi.org/10.1039/c1cp20722a
83. G. Bitencourt-Ferreira and W.F. De Azevedo Jr., *Methods Mol. Biol.*, **2053**, 149 (2019); https://doi.org/10.1007/978-1-4939-9752-7_10
84. D. Pathak, N. Chadha and O. Silakari, *J. Mol. Graph. Model.*, **70**, 85 (2016); https://doi.org/10.1016/j.jmgm.2016.09.013
85. H.V. Sanghani, S.H. Ganatra and R. Pande, *J. Comput. Sci. Syst. Biol.*, **05**, (2012); https://doi.org/10.4172/jcsb.1000085
86. B. Silvi and A. Savin, *Nature*, **371**, 683 (1994); https://doi.org/10.1038/371683a0
87. G. Xiong, Z. Wu, J. Yi, L. Fu, Z. Yang, C. Hsieh, M. Yin, X. Zeng, C. Wu, A. Lu, X. Chen, T. Hou and D. Cao, *Nucleic Acids Res.*, **49(W1)**, W5 (2021); https://doi.org/10.1093/nar/gkab255
88. V. Polshettiwar, R.S. Varma, *Green Chem.*, **12**, 743 (2010); https://doi.org/10.1039/b921171c
89. K. Hartonen, M.L. Riekkola, *Elsevier eBooks*, 19–55 (2017).
90. B.S. Furniss, A.J. Hannaford, P.W.G. Smith and A.R. Tatchell, Vogel's Text Book of Practical Organic Chemistry, Longman: New York, edn. 5 (1989).
91. S. Santosh Kumar, K.I. Priyadarsini and K.B. Sainis, *Redox Rep.*, **7**, 35 (2002); https://doi.org/10.1179/135100002125000163
92. M. Singhal, A. Paul, H.P. Singh, S.K. Dubey and K. Gaur, *J. Chem. Pharm. Res.*, **3**, 639 (2011).
93. R.J. Ouellette and J.D. Rawn, Principles of Organic Chemistry, Elsevier eBooks, edn. 2, pp. 51–86 (2018).
94. C. Zheng and O. Rubel, *J. Phys. Chem. C*, **121**, 11977 (2017); https://doi.org/10.1021/acs.jpcc.7b00333
95. B. Ahmed, P. Barukial and B. Bezbaruah, *J. Indian Chem. Soc.*, **100**, 101027 (2023); https://doi.org/10.1016/j.jics.2023.101027
96. A. Daina and V. Zoete, *ChemMedChem*, **11**, 1117 (2016); https://doi.org/10.1002/cmdc.201600182
97. R.C. Braga, V.M. Alves, M.F.B. Silva, E. Muratov, D. Fourches, L.M. Lião, A. Tropsha and C.H. Andrade, *Mol. Inform.*, **34**, 698 (2015); https://doi.org/10.1002/minf.201500040